Molecular Dynamics Simulation Studies of the Hydrogen Bond Network in Water

ALFONS GEIGER AND PETER MAUSBACH

Fachbereich Chemie der Universität Dortmund;
Otto-Hahn-Str., D-4600 Dortmund, West-Germany
and
Institut für Physikalische Chemie der RWTH Aachen;
Templergraben 59,D-4600 Dortmund, West-Germany

1 Introduction

It is generally accepted that the unusual properties of water are largely due to the structure and dynamics of its hydrogen-bond network [1,2,3]. There has been much speculation about its connectivity pattern, but unfortunately there is no possibility to observe the hydrogen-bond network directly by experiments. This dilemma can be overcome by using realistic computer simulations [4]. Such calculations reveal the picture of an infinite random network, which is subject to continuous and rapid restructuring [5]. Fig. 1 gives a characteristic grafical representation of the hydrogen-bond network, obtained from a molecular dynamics simulation.

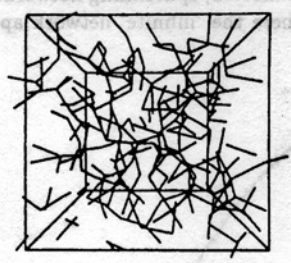

Figure 1: Illustration of the hydrogen-bond network. Configuration of 216 water molecules in a periodic box.

It is possible to describe the connectivity of this random network quantitatively by using lattice percolation theory [6,7,14]. By studying the changes that are produced by varying temperature and density, one can contribute to the understanding of various effects observed in metastable water and aqueous solutions.

J.C. Dore and J. Teixeira (eds.), Hydrogen-Bonded Liquids, 171–183.

2 Molecular dynamics simulations outline

In the following, we discuss the results of two series of molecular dynamics simulations. In one series, the density is kept fixed at $\varrho = 1.0 g/cm^3$ and the temperature is varied in eight steps from 287 to 235 K. In the other, at an approximately constant temperature of T = 273 K, the density is varied stepwise from $\varrho = 1.0 g/cm^3$ to $0.7 g/cm^3$.

We compare the results of these 'supercooling' and 'stretching' series with a simulation of 'normal' water at $\varrho = 1.0 g/cm^3$ and T = 284 K. In all cases we performed constant energy and constant density (N,V,E) simulations [8] for systems of 216 water molecules which interact via an ST2 pair potential [9]. The direct molecular interactions up to the cutoff distance $r_c = 7.8 \AA$ were combined with a reaction field approximation for more distant parts of the system [10]. Before the actual simulations were started, equilibration runs were applied, which extended up to 300 ps as the systems became more viscous with decreasing temperature or density. For more details see refs. [11] and [12].

3 Hydrogen-bond definition

The interaction of water molecules is described by a continuous potential surface, which does not allow us to distinguish naturally between 'broken' and 'intact' hydrogen bonds. It is more appropriate to think of a smooth unimodal distribution of strong, weak and non-existing hydrogen bonds. To treat such systems with traditional bond percolation theory [2,13], where an unambiguous definition of an intact bond is necessary, the following approach has proven to be very successful.

To start, a reasonable and practicable definition is imposed: two molecules i and j are considered to be hydrogen-bonded whenever their interaction energy V_{ij} is below a negative threshold value V_{HB} and their mutual oxygen-oxygen separation is less than 3.5 Å. The arbitrary value V_{HB} is then varied gradually from strongly negative values, close to the absolute minimum of the interaction potential, up to values close to zero [5,7]. In this way, we can observe the connectivity pattern produced by the strongest bonds and the growth of the network, as weaker and weaker bonds are included.

First, only few bonds will be found, the average number of hydrogen-bonds per water molecule n_{HB} will be close to zero, and only very small aggregates of connected molecules will be observed. With increasing (less negative) V_{HB}, n_{HB} will increase, as will the number of the hydrogen-bonded aggregates and their average size S. When V_{HB} approaches zero, n_{HB} approaches values close to four; the bonds will then form a totally connected, spacefilling network. At some intermediate value of V_{HB} a bond percolation threshold, where the 'infinite' network appears for the first time, will have been passed.

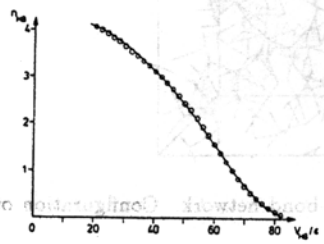

Figure 2: Average number of hydrogen-bonds n_{HB} per water molecule as function of energy threshold V_{HB}.

A quantitative description of the behaviour outlined above is given in the following figures for

the system at T = 284 K and $\varrho = 1.0 g/cm^3$. Fig. 2 shows n_{HB} as a function of the threshold value V_{HB} in units of the ST2-parameter $\epsilon = 0.317 J/mole$.

As one can see, for very strict definitions only few (strong) hydrogen-bonds are found, whereas for V_{HB} values close to zero n_{HB} even exceeds the value of four which one expects from crystalline ice. This indicates the presence of 'bifurcated' H-bonds, at least according to the above definition and if weak bonds are also considered.

4 Hydrogen-bonds in normal water

Assuming independent forming and breaking of H-bonds on a lattice of four-bonded water molecules, one expects a mole fraction of

$$f_j = \binom{4}{j} p_j (1-p)^{4-j} \tag{1}$$

water molecules, which have exactly j bonds. p is the bond forming probability.

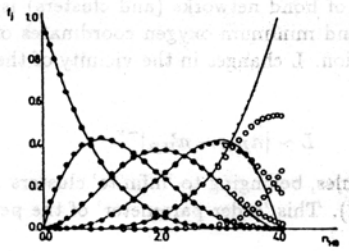

Figure 3: Fraction f_j of water molecules with j intact H-bonds (j = 0 ... 5). Circles: MD results, full line: binomial distribution.

In Fig. 3 the circles show values of f_j, obtained from the MD simulation for various choices of V_{HB}, plotted against the average number of H-bonds n_{HB} (V_{HB}). The full lines represent the binomial distribution, eq. (1), with $p = n_{HB}/4$. Up to $n_{HB} \approx 3$, one observes very good agreement, whereas for larger n_{HB}, when weak H-bonds are also permitted, increasing deviations are observed. This is due to the appearance of five-bonded water molecules.

In a next step, we study larger molecular aggregates. We distinguish between bond-*networks* of water molecules and aggregations of four-bonded molecules, which we call *clusters*. As the assumption of independent breaking of bonds on an ice lattice works well for f_j, the occurance probability of small to medium-sized networks and clusters can be calculated by combination theory [3]. As an example, the probability of finding clusters of *three* connected four-bonded molecules (weight fraction of water molecules, belonging to such clusters) is given by

$$W_3^c = 18 p^{10} (1-p^3)^8 \tag{2}$$

and the corresponding values from the simulation are compared in Fig. 4.

The plot is equivalent to Fig. 3, with $p = n_{HB}(V_{HB})/4$. Again, a very good agreement is observed, although a small but systematic deviation is present, which will be discussed later. The bell shape of the curve, which one observes for all W_n, can be understood as follows: Starting with a very strict definition and gradually relaxing it, we find at first few aggregates of a given size n, which multiply with increasing $n_{HB}(V_{HB})$. Finally, there will be many of these networks and clusters, which start to merge, thus decreasing again W_n.

When approaching the percolation threshold, the size of the aggregates increases strongly. For large aggregates the probability W_n can no more be given analytically (at least, when an underlieing

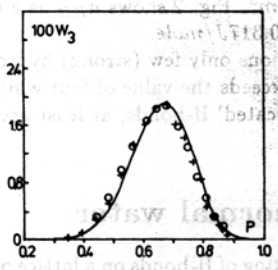

Figure 4: Fraction W_3^c of water molecules, which belong to clusters of three four-bonded molecules.

ice lattice topology is assumed), but close to the percolation point, the average network or cluster size and related properties can be described by critical behavior type equations. As an example in Fig. 5a the 'spanning length' L of bond networks (and clusters) is shown. L is defined as the difference between the maximum and minimum oxygen coordinates of the networks with respect to some arbitrary coordinate direction. L changes in the vicinity of the percolation threshold n_{HB}^* like

$$L \sim |n_{HB} - n_{HB}^*|^{-\nu}. \tag{3}$$

In Fig. 5b the fraction of molecules, belonging to 'infinite' clusters P_∞ is shown for two slightly different H-bond definitions (see [6]). This 'order parameter' of the percolation transition behaves like

$$P_\infty \sim |n_{HB} - n_{HB}^*|^{\beta}. \tag{4}$$

In accord with lattice percolation theory, we can use for n_{HB}^* the values 1.55 and 3.18 for networks and clusters respectively. The straight lines in Figs. 5a,b have been drawn with a slope

$$\begin{aligned} \nu &= 0.75 \\ \text{and } \beta &= 0.38, \end{aligned}$$

as predicted by lattice percolation theory [6]. The very good fit of the simulation data is obvious.

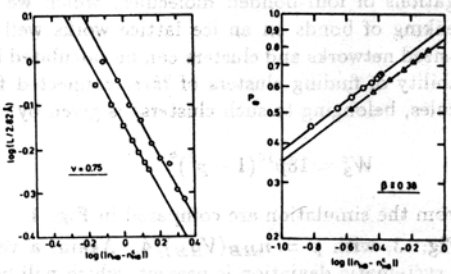

Figure 5: (a) Average length of bond networks and clusters. (b) Fraction of molecules which belong to spanning clusters.

The ramified networks close to the percolation threshold can be described as fractals, which means that the mass distribution in a percolating network is such that the number of particles N, which are found within a sphere of radius r around some reference particle is

$$N(r) \sim r^{d_f}. \tag{5}$$

A so called 'hyperscaling hypothesis' suggests for the fractal dimension d_f a value which is determined by the discussed critical exponents (D=3 is the Euclidian dimension) [13]:

$$d_f = D - \beta/\nu. \tag{6}$$

With the values given above, we expect $d_f = 2.49$. To determine d_f via eq. (5), systems of 216 particles are not sufficient. Therefore we simulated a system of 1728 water molecules, but even with this size only a hint for the appropriateness of eq. (6) can be given [26].

In Fig. 6a, the derivative of N(r) viz. the average number of molecules c(r) within spherical shells is shown for networks of size 850 to 900 close to the bond percolation threshold $n^c_{HB} = 1.55$. To remedy the limitations of our finite size system, we determine the slope $d_f - 1$ for various network sizes N and plot d_f vs. N^{-1}. Fig. 6b reveals that our results from a finite system simulation at least do not contradict the prediction of eq. (6).

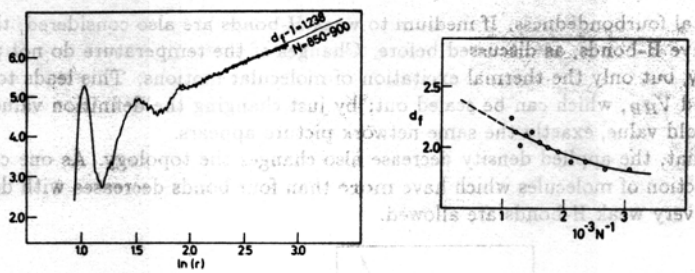

Figure 6: (a) Radial distribution c(r) of water molecules, which belong to same network. (b) Fractal dimension: slope $d_f - 1$ for various network sizes N.

5 Temperature and density dependence of hydrogen-bond network topology.

Fig. 4a revealed very small, but systematic deviations between the prediction from combination theory and the MD results. Now we discuss possible reasons for these deviations. As an example we plot in Fig. 7 these differences for the previously discussed clusters of size three:

$$\Delta W^c_3(p) = W^c_3(p) - W^c_{3,MD}(p) \tag{7}$$

where $W^c_3(p)$ is given by eq. (2) and $W^c_{3,MD}(p)$ are the MD values.

An important difference between the pure temperature effect at constant density (Fig. 7a), and the pure density effect at constant temperature (Fig. 7b) can be seen. The influence of the temperature can be scaled out: by plotting vs. the average number of H-bonds, all difference curves fall on top of each other. In contrast, the difference ΔW_n diminishes with decreasing density and seems to vanish over the total range of p within the given numerical accuracy at $\varrho \approx 0.8 g/cm^3$. Of course, the average number of H-bonds changes (increases) with decreasing temperature and density [11,12], and by that also the occurance probability of the networks, but apparently this effect can be scaled out in one case, but not in the other.

This can be explained as follows: the observed differences occure, because the topology of the H-bond network in the liquid is not the ice lattice topology, and in particular, there are deviations

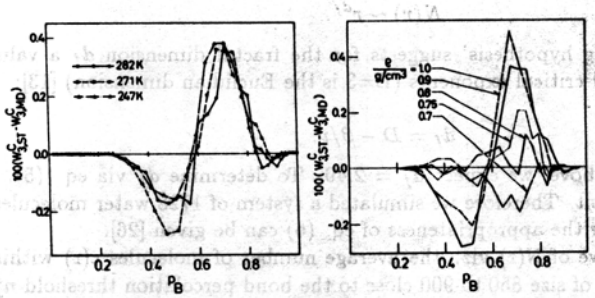

Figure 7: Difference between cluster size distribution in MD simulation and prediction of percolation theory (a) temperature dependence, (b) density dependence.

from the perfect local fourbondedness. If medium to weak H-bonds are also considered, there may be molecules with five H-bonds, as discussed before. Changes of the temperature do not primarily change the topology, but only the thermal excitation of molecular motions. This leads to changes in p and W_n at fixed V_{HB}, which can be scaled out: by just changing the definition value V_{HB} to bring p back to its old value, exactly the same network picture appears.

In contrast to that, the applied density decrease also changes the topology. As one can see in Fig. 8, the mole fraction of molecules which have more than four bonds decreases with decreasing density, even when very weak H-bonds are allowed.

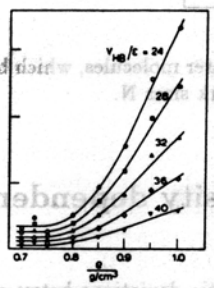

Figure 8: Mole fraction of water molecules with more than four H-bonds (for various H-bond definitions).

The local connectivity approaches a more perfect tetrafunctional local arrangement (as assumed for the derivation of the W_n [7]).

6 Structure of low density metastable water

In the previous section, only topological properties of the H-bond network have been discussed. We now consider the structural (geometrical) changes, which are observed as density decreases. This is of special interest, because of a conjectured limit of stability (spinodal) of 'stretched' water [15], which was estimated to be at a negative pressure of roughly -200 MPa and a density of $\varrho \approx 0.8 g/cm^3$ for the temperature of our simulation series ($T \approx 273K$).

In fact, there are a number of observations which indicate the disintegration of the bulk water system at the above given conditions. Fig. 10 gives the virial, calculated from the pair interaction forces (without cutoff correction). A decrease of the pressure at high densities ends at a pressure of about -200 MPa, when the density $0.75 g/cm^3$ is reached. Although these numbers can only be

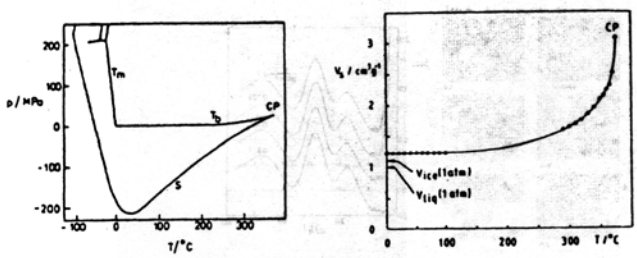

Figure 9: (a) Line of mechanical stability limit for metastable water, (b) specific volume at the limit of stability. Both according to Speedy [15].

considered as rough estimates, they are consistent with Speedy's conjecture [15].

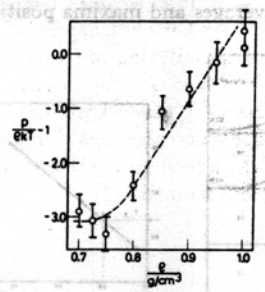

Figure 10: Decrease of pressure virial with density.

Fig. 11a gives a graphical description of the local density fluctuations in water at different global densities ϱ. To get these pictures, the simulation box is cross-sectioned by an arbitrarily positioned, finely meshed plane. Then, each mesh point, which is closer than $2.5\mathring{A}$ to any water oxygen in the system is marked by a cross. Thus the empty white areas in Fig. 11a indicate cavities in the water. As one can see, between 1.0 and $0.8g/cm^3$ the decreasing global density produces more, but not larger cavities. But below $0.8g/cm^3$ very large cavities occure, indicating the tendency for decomposition. The presence of these large scale density fluctuations can be proven by calculating the static structure factor

$$S(\mathbf{Q}) = \frac{1}{N} < \sum_{i,j} exp(i\mathbf{Q}\mathbf{R}_{ij}) > \qquad (8)$$

where $\mathbf{R}_{ij}$ is the oxygen distance vector between molecules i and j. For scattering vectors with $|\mathbf{Q}| \geq 1.2\mathring{A}^{-1}$, S(Q) has been calculated by Fourier-transforming the oxygen pair correlation function $g_{OO}(r)$ (see Fig. 13a). For smaller Q-values S(Q) is calculated directly from the sum in eq. (8). The smallest accessible wave vector is $Q_1 = 2\pi/L$, where L is the simulation box size, which varies between 18.6 and 21.0 $\mathring{A}^{-1}$ for the different densities. As one can see from Fig. 11b, for densities below $0.8g/cm^3$ a strong increase at small Q-values indicates the presence of large scale density fluctuations.

The transition point from a homogeneous to a decomposing system with large density fluctuations can be localized by considering the Voronoi polyhedra [17,16] which are obtained by using the oxygens to describe the positions of the water molecules. Such Voronoi constructions are spacefilling and uniquely partition the total volume between the molecules. Fig. 12a gives the distributions

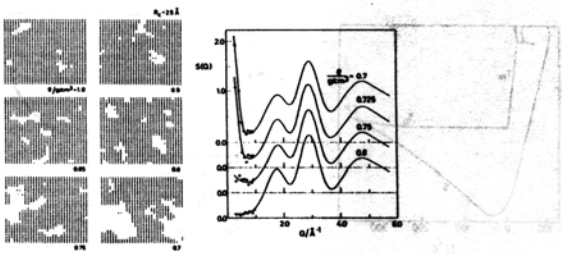

Figure 11: (a) Picture of the density fluctuations in low density water. (b) Structure factor S(Q).

of the Voronoi cell volumes at various densities. For higher densities these bell shaped curves are symmetric. The maxima coincide with the averages (first moments) of the distributions and as the Voronoi construction is spacefilling, the average shifts proportional to the global density chang (see Fig. 12b, crosses and circles for averages and maxima positions, respectively).

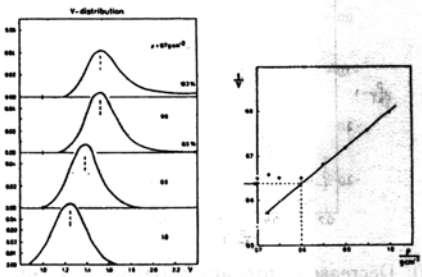

Figure 12: (a) Volume distribution of Voronoi polyhedra. (b) Maximum position (o) and mean value (+) of Voronoi distribution.

Below $0.8g/cm^3$ the volume distribution becomes very unsymmetric, because polyhedra of large size are occuring. These belong to molecules which are in the neighborhood of the large cavities. At these low densities, a global density decrease only enlarges these cavities, but leaves the density of the 'bulk' unchanged. Therefore the maximum does not shift further. Thus, the divergence of first moment and maximum position indicates the decomposition of the system into a 'bulk' phase and cavities [18]. This begins at $\varrho \approx 0.8g/cm^3$, as one can see from Fig. 12b.

To understand the mechanisms that lead to the decomposition at this particular density $\varrho \approx 0.8g/cm^3$, we determine the number of first neighbors $N(R_1)$ by integrating over the first peak of the oxygen-oxygen pair distribution function (Fig. 13a). Note, that the change of $g_{OO}(r)$ with density is very unusual: the oscillations of $g_{OO}(r)$ become more pronounced and in particular the height of the first peak increases with decreasing density. This demonstrates the development of a more ordered structure with decreasing density. Also, the slight shift of the second peak to larger distances indicates the formation of more linear hydrogen bonds.

It is well known that in the liquid at $1.0g/cm^3$ the water molecule has more than four nearest neighbors (of course, the actual number depends on the upper integration limit). The shape of $N(R_1)$, as shown in Fig. 13b, shows the same density dependence as the maximum positions of the Voronoi volume distribution (Fig. 12b) and the mole fraction of water molecules with more than four H-bonds (Fig. 8). Above and below $0.8g/cm^3$ the system reacts with two very different mechanisms upon an imposed density decrease. Above $0.8g/cm^3$ a global density decrease is achieved by reducing the number of nearest neighbors. At about $0.8g/cm^3$ a more ordered

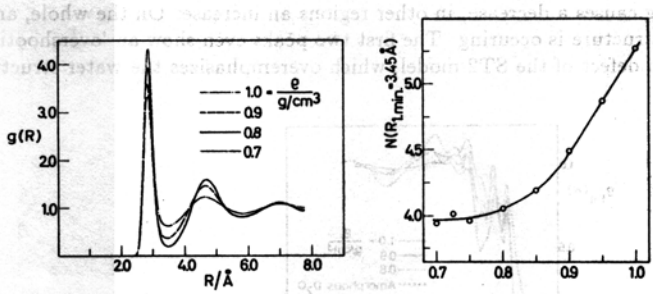

Figure 13: (a) Oxygen-Oxygen pair distribution function in low density water, (b) number of nearest neighbors.

ructure with four nearest neighbors per water molecule is reached (see also the discussion of Fig. 7b). A further reduction of the density is then achieved by the formation of large holes. This is energetically more favourable than to loosen the hydrogen-bonding interaction to one of the four remaining nearest neighbors: By adopting a 'straddling' orientation towards the cavity [12] (as this is also known from hydrophobic hydration shells [19]), the water molecules are able to keep four H-bonded neighbors, while reducing the density globally by the formation of cavities.

It is quite comprehensible that at this stage the system becomes very unstable with respect to density fluctuations. This is a simple explanation for the location of the mechanical stability limit at $\varrho = 0.8 g/cm^3$, as suggested by Speedy [15].

In Fig. 14 the oxygen-hydrogen and hydrogen-hydrogen pair correlation functions $g_{OH}(r)$ and $g_{HH}(r)$ are shown. The prominent peaks are characteristic for water and are produced by the mutual arrangement of H-bonded molecules [9]. With decreasing density we observe again a more pronounced structural order. In particular the first peak of $g_{OH}(r)$, which corresponds to the distance between the hydrogen in the H-bond and its acceptor oxygen, increases very rapidly and the following minimum is lowered accordingly.

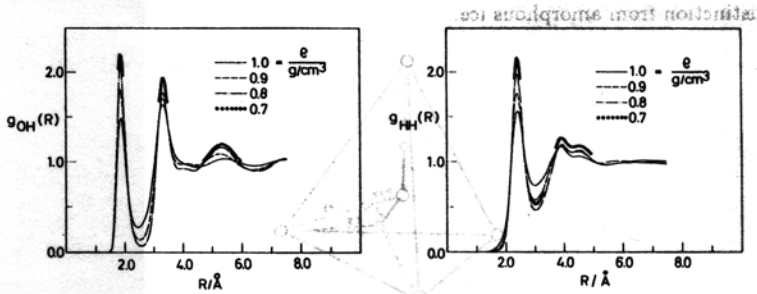

Figure 14: Intermolecular pair distribution functions in low density water: (a) oxygen-hydrogen, (b) hydrogen-hydrogen.

With neutron diffraction experiments on D_2O, a weighted sum of the shown pair correlation functions can be determined (assuming structural equivalence of H and D):

$$g_{tot}(r) = 0.092 g_{OO}(r) + 0.422 g_{OH}(r) + 0.486 g_{HH}(r). \quad (9)$$

These sums are shown in Fig. 15 and compared with a neutron scattering result for amorphous D_2O of Chowdhury et al. [21]. It turns out that the changes caused by the expansion of the water are comparable to those observed in n-scattering experiments on undercooled water [20]: In those regions, where $g_{tot}(r)$ of the amorphous ice is lower than in the liquid (for example at about $3\mathring{A}$),

stretching or cooling causes a decrease, in other regions an increase. On the whole, an approach to the amorphous ice structure is occuring. The first two peaks even show an 'overshooting', probably due to a well-known defect of the ST2 model, which overemphasizes the water structure.

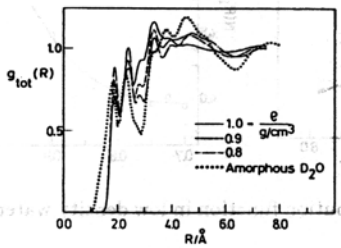

Figure 15: Weighted sum of pair correlation functions from MD compared with neutron-scattering results of amorphous ice.

Following a proposition of Giguère [22], which had been taken up by Dore to interpret the n-scattering results [20], a very simple and grafic explanation for the discussed changes can be given. At higher densities and temperatures an appreciable amount of local arrangements occure, where the hydroxyl group is pointing between the oxygens of two neighbouring water molecules as drawn in Fig. 16 [22]. This transient arrangement, which may be called a bifurcated H-bond, can be fitted in the overall tetrahedral network and corresponds to O-H distances of 2.3 rather than 1.85Å. Accordingly, the increase of the first peak of $g_{OH}(r)$ and the simultaneous depletion of the following minimum indicates a strong reduction of bifurcated H-bonds and is in perfect agreement with our previous observations like the disappearance of five-bonded water molecules (Fig. 8).

It has to be stressed that the term 'bifurcated H-bond' is used here in the above described energetic or geometric sense. It seems that using a hydrogen-bond definition which incorporates also the lifetime [14], such arrangements can no longer be addressed as bonds. Nevertheless, such configurations, even though only transient, are characteristic for liquid water and its structural and dynamical distinction from amorphous ice.

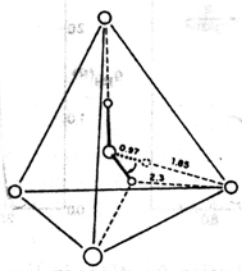

Figure 16: 'Bifurcated H-bond' arrangement. According to Giguère [22].

7 Hydrogen-bonding and microdynamics

The dynamics of the water molecules in the expanded liquid also reveals a density dependence which is completely diverse to what is expected from 'normal' liquids. Usually, expansion increases the molecular mobility, due to reduced steric hindrance. In contrast to this, in water a drastic reduction of molecular mobility is observed, even at small density decreases (and at constant temperature).

In ref. [12] we discussed the mean square displacements $< \Delta r^2(t) >$ and the corresponding self diffusion coefficients D: A density decrease of 20 % (from 1.0 to $0.8 g/cm^3$) produces a reduction of D by nearly a factor of 10! An analogueous behavior can be observed when considering the reorientational motion of the molecules. Here we calculate the time correlation functions

$$T_l(t) =< P_l(\cos\theta(t)) >,$$

where P_l is the Legendre Polynomial of degree l and

$$\cos\theta(t) = \hat{l}_i(0) \cdot \hat{l}_i(t)$$

describes the rotation of a molecule fixed unit vector $\hat{l}_i$. The correlation time τ_l is defined as

$$\tau_l = \int_0^\infty T_l(t)\, dt.$$

As an example, the density dependence of $T_2(t)$ and τ_2 of the intramolecular H-H-vector is shown in Fig. 17a. For the integration to obtain τ_l, $T_l(t)$ is extrapolated to infinity by an exponential function. The very rapid initial decay of $T_l(t)$ is due to the well-known librational (hindered rotational) motion of the water molecules. With decreasing density, the librational amplitude is slightly diminished and the following exponential decay is slowed down considerably. Accordingly the reorientation times τ_l increase until a plateau is reached at about $0.8 g/cm^3$ (Fig. 17b).

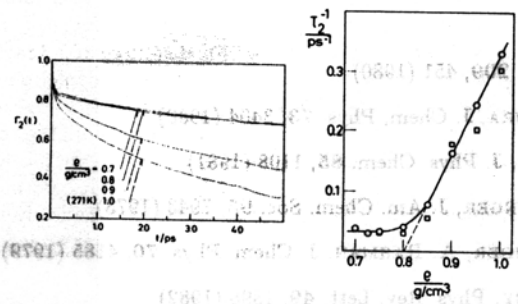

Figure 17: Density dependence of reorientational correlation functions and corresponding correlation times.

A mechanism, which allows us to understand this loss of mobility, has been proposed by Naberukhin [23] in correspondence with the structural considerations of Giguère [22], which we discussed above. Accordingly, the mobility of the water molecules is strongly influenced by the presence of 'bifurcated H-bonds'. Structures which comprise many local arrangements of the kind discussed in Fig. 16, reflect a facilitated switching from one 'regular' H-bond arrangement to another, across lowered energy barrieres. The structural changes observed in Figs. 8 and 14 reflect the disappearance of such 'bifurcated H-bonds' (*defects* of the tetra-functional bond network) and explain the observed loss of mobility.

8 Conclusions

We have shown that the *connectivity* of the hydrogen-bond network can be described quite well by random bond percolation on a lattice. It has also been shown that the *structure* of amorphous ice can be represented by so called continuous random network models, developped for amorphous semiconductors [3,20,24]. A close inspection of the stretched liquid revealed however that the deviations of the structure from the 'ideal' tetra-functional network with four neighbors and

four bonding-possibilities per molecule are very important for the properties of water. The ideal tetrahedral network structure is attained only at the mechanical stability limit, which thus can be identified with a new kind of order transition (with the quantities shown in Figs. 8 and 13b as order parameter).

In retrospect, the high mobility of the water molecules seems to be in contradiction to the results of the percolation study, that at any instance a spanning network of strong H-bonds ($V_{ij} \leq -18$ kJ/mole) is present. In view of the fact that this interaction energy is large compared to the thermal energy kT, one should expect water to be gel-like, at least highly viscous. In fact this can be observed in the simulation at low densities.

Therefore, the deviations from a perfect tetrahedral network are of decisive importance for the molecular dynamics. Random network models which focus on distorted tetrahedral local order without considering explicitely arrangements of five nearest neighbors habe to be re-examined under this point of view.

There are experimental observations, which perfectly support our findings regarding low density water: the hydrophobic hydration effect. It is well-known that inert solutes produce increased structural order and decreased mobility in its hydration shell [19,25]. This can easily be understood by realizing that the main effect of the inert solute is to lower *locally* the density of water and to prevent the 'straddling' tetrahedral arrangement (see [19]) of the water molecules in the first hydration shell from being disturbed by the approach of 'fifth neighbors'.

References

[1] F.H. Stillinger, Science **209**, 451 (1980)

[2] H.E. Stanley, J. Teixeira, J. Chem. Phys. **73**, 3404 (1980)

[3] S.A. Rice, M.G. Sceats, J. Phys. Chem. **85**, 1108 (1981)

[4] A. Rahman, F.H. Stillinger, J. Am. Chem. Soc. **95**, 7943 (1973)

[5] A. Geiger, F.H. Stillinger, A. Rahman, J. Chem. Phys. **70**, 4185 (1979)

[6] A. Geiger, H.E. Stanley, Phys. Rev. Lett. **49**, 1895 (1982)

[7] R.L. Blumberg, H.E. Stanley, A. Geiger, P. Mausbach, J. Chem. Phys. **80**, 5230 (1984)

[8] M.P. Allen, D.J. Tildesley, "Computer Simulation of Liquids", Clarendon Press, Oxford 1987

[9] F.H. Stillinger, A. Rahman, J. Chem. Phys. **60**, 1545 (1974)

[10] O. Steinhauser, Mol. Phys. **45**, 335 (1982)

[11] A. Geiger, P. Mausbach, J. Schnitker, R.L. Blumberg, H.E. Stanley, J. Physique Colloq. **45**, C7-13 (1984)

[12] A. Geiger, P. Mausbach, J. Schnitker, in "Water and Aqueous Solutions", ed. G.W. Neilson and J.E. Enderby: Adam Hilger, Bristol 1986

[13] D. Stauffer, "Introduction to Percolation Theory", Taylor and Francis, London 1985

[14] F. Sciortino, S.L. Fornili, J. Chem. Phys. **90**, 2786 (1989)

[15] R.J. Speedy, J. Phys. Chem. **86**, 982 (1982)

[16] N.N. MEDVEDEV, V.P. VOLOSHIN, YU.I. NABERUKHIN, J. Phys. A: Math. Gen. **21**, L247 (1988)

[17] N.N. MEDVEDEV, J. Computat. Phys. **67**, 223 (1986)

[18] N.N. MEDVEDEV, A. GEIGER, to be published

[19] A. GEIGER, A. RAHMAN, F.H. STILLINGER, J. Chem. Phys. **70**, 263 (1979)

[20] J.C. DORE, in "Water Science Reviews", Vol. 1, ed. F. FRANKS, University Press, Cambridge 1985

[21] M.R. CHOWDHURY, J.C. DORE, J.T. WENZEL, J. Non-Cryst. Solids **53**, 247 (1982)

[22] P.A. GIGUÈRE, J. Chem. Phys. **87**, 4835 (1987)

[23] YU.I. NABERUKHIN, J. Struct. Chem. **25**, 223 (1984)

[24] M. POPESCU, J. Non-Cryst. Solids **75**, 483 (1985)

[25] A. GEIGER, Ber. Bunsenges. Phys. Chemie **85**, 52 (1981)

[26] P. MAUSBACH, A. GEIGER, Z. angew. Math. Mech. **69**, T55 (1989)